Acta Biomaterialia 7 (2011) 1192–1201

Contents lists available at ScienceDirect

Acta Biomaterialia

journal homepage: www.elsevier.com/locate/actabiomat

# Regeneration of the femoral epicondyle on calcium-binding silk scaffolds developed using transgenic silk fibroin produced by transgenic silkworm

Aya Nagano [a,b], Yumi Tanioka [a], Nobuko Sakurai [b], Hideki Sezutsu [c], Noboru Kuboyama [d], Hideo Kiba [d], Yasuhiro Tanimoto [d], Norihiro Nishiyama [d], Tetsuo Asakura [a,*]

[a] Department of Biotechnology, Tokyo University of Agriculture and Technology, Koganei, Tokyo 184-8588, Japan
[b] Research Department, Japan Medical Materials Corporation, Osaka 532-0003, Japan
[c] National Institute of Agribiological Science, Tsukuba, Ibaraki 305-8602, Japan
[d] Nihon University School of Dentistry at Matsudo, Matsudo, Chiba 271-8587, Japan

ARTICLE INFO

*Article history:*
Received 7 June 2010
Received in revised form 21 October 2010
Accepted 28 October 2010
Available online 3 November 2010

*Keywords:*
Bone regeneration
Calcium binding activity
Silk fibroin
Scaffold
Transgenic silkworm

ABSTRACT

Genetically modified silk fibroin containing a poly-glutamic acid site, $[(AGSGAG)_4E_8AS]_4$, for mineralization was produced as fibers by transgenic silkworms through systematic transformation of the silkworms. The Ca binding activity and mineralization of the transgenic silk fibroin were examined in vitro, showing that this transgenic silk fibroin had relatively high Ca binding activity compared with native silk fibroin. Porous silk scaffolds were prepared with the transgenic and native silk fibroins. Healing of femoral epicondyle defects in rabbit femurs treated with the scaffolds was examined by observing changes in images of the defects using micro-computed tomography. Earlier mineralization and bone formation were observed with scaffolds of transgenic silk fibroin compared with those of native silk fibroin. Thus, this study shows the feasibility of using genetically modified silk fibroin from transgenic silkworms as a mineralization-accelerating material for bone repair.



## 1. Introduction

The clinical need for materials for bone regeneration is expected to increase. Currently, close to 1000,000 bone grafts are performed each year for skeletal augmentation [1–3]. Autografts remain the clinical standard for bone repair because they involve use of the patient's own cells and growth factors, however, issues of donor site morbidity and prolonged hospitalization remain to be overcome [4]. Further, allografts carry the risks of immune rejection and disease transmission [5]. Orthopedic procedures would, therefore, benefit from osteopromotive scaffolds that could be used to provide a space for tissue organization, enhance migration, and deliver osteogenic cells and cytokines. These materials should have essential characteristics, including biocompatibility, porosity, and appropriate mechanical properties.

Some polymeric scaffolds have been examined, but issues regarding these scaffolds remain unresolved, such as the poor mechanical properties of collagen and inflammation caused by acidic hydrolysis products of poly(lactic–co-glycolic acid) or poly-L-lactic acid [6]. In contrast, silk fibroin from *Bombyx mori* has superior mechanical properties that are tailorable: they degrade slowly, permitting an adequate time for remodeling, and they are biocompatible. Many studies have demonstrated the feasibility of *B. mori* silk fibroin-based porous scaffolds [7–14], many of which drive successful bone repair by providing bone marrow stem cells [7–10,12,13] or osteoblast-like cells [11]. However, the primary structure of *B. mori* silk fibroin is a highly repetitive sequence, $(Ala\text{-}Gly\text{-}Ser\text{-}Gly\text{-}Ala\text{-}Gly)_n$ [15], which does not have enough Ca-binding sites for mineralization. Previous studies have reported that mineralization on silk fibroin scaffolds is needed for osteoconductivity in the presence and absence of cells [7–10,12,13].

The mineralization process is naturally induced in native bone by self-assembly at the charged acidic domains of non-collagenous proteins, which provide adequate conditions for the nucleation of calcium hydroxyapatite (HAP) and development of ordered HAP crystals [16–26]. These activities can be mimicked in vitro by synthetic homopolymers or proteins containing with poly-L-glutamic acid [27]. These finding focus on poly-L-glutamic acid as the HAP nuclei-forming sites in proteins. In previous studies we have mimicked the self-assembly system in native bone [28,29]. A new strategy for bone repair was advanced by using the sequence $[(AGSGAG)_4E_8AS]_4$, which combines the excellent mechanical properties of the *B. mori* silk fibroin repetitive domain $(AGSGAG)_n$ and the Ca binding properties of the poly-glutamic acid domain.

In the present study transgenic silk fibroin containing the Ca binding sequence $[(AGSGAG)_4E_8AS]_4$ is produced as fibers, through the systematic transformation of silkworms [30–32]. The Ca binding activity and mineralization of the transgenic silk fibroin is examined

* Corresponding author. Tel.: +81 42 388 7025; fax: +81 42 388 7733.
*E-mail address:* asakura@cc.tuat.ac.jp (T. Asakura).

1742-7061/$ - see front matter © 2010 Acta Materialia Inc. Published by Elsevier Ltd. All rights reserved.
doi:10.1016/j.actbio.2010.10.032

in vitro. Then we build on those studies by implanting the porous silk scaffolds into rabbit femurs in vivo. Healing of femoral epicondyle defects is examined by observing changes in the images of defects using micro-computed tomography (micro-CT). Thus we develop new Ca binding porous silk scaffolds with transgenic silk fibroin for bone repair.

## 2. Materials and methods

### 2.1. Construction of the transgenic silkworm

Multimerized DNA fragments of the $[(AGSGAG)_4E_8AS]_4$ sequence were obtained by a method previously used to produce transgenic silk fibroin [30–32]. Oligonucleotide fragments encoding the crystalline region of *B. mori* silk fibroin and poly-glutamic acid, the Ca binding region, are shown in Fig. 1a. Each fragment was inserted into an *Spe*I- and *Nhe*I-digested pUC118 linker to construct the monomer of transgenic silk fibroin. Multimers of the sequence $(AGSGAG)_4E_8AS$ were obtained using previous strategies that involved head to tail ligation and orientation for *Nhe*I and *Spe*I sites [30–32]. Multimerized DNA fragments encoding these recombinant proteins were inserted into the *Bam*HI- and *Hin*dIII-digested expression vector pET30a.

Transgenic silkworms were constructed as described previously [30–32]. A transformation vector, piggy Bac-3xP3 DsRed-H pro-$(AGSGAG)_4E_8$, was designed to produce recombinant silk fibroin that contained the fused gene with fibroin heavy (H)-chain cDNA, $(AGSGAG)_4E_8$, and green fluorescent protein (GFP) sequences. *Escherichia coli* DH5a was used as the host strain. A schematic for the construction of plasmids is shown in Fig. 1b. Two oligonucleotides, 5′-AGCTAAGATCTC-3′ and 5′-TTCTAGAGTCGA-3′, were used as linkers to construct the *Bgl*II restriction site, which was used to introduce $(AGSGAG)_4E_8$ into the *Bam*HI sites of pHC-EGFP 24. After pET30a tetramers were digested with *Bam*HI and *Bgl*II, the fragments were inserted into *Bam*HI-digested pHC-EGFP. After pHC-$(AGSGAG)_4E_8$-EGFP was digested with *Asc*I and *Fsc*I, the fragments were inserted into *Asc*I/*Fsc*I-digested pBac [3xP3-DsRed/EGFP afm] (Fig. 1b and c). The plasmid was transformed into *E. coli* J109.

To construct transgenic silkworms, plasmid DNA was injected into 550 eggs of the w1-pnd strain in the pre-blastodermal stage (Fig. 1d). Transgenic insects were screened for the expression of DsRed in the stemmata of $G_1$ embryos, under a fluorescence microscope (Leica, Tokyo, Japan) equipped with a filter set for DsRed. The GFP fluorescence of the silk gland was observed under a microscope equipped with a filter set for GFP (Fig. 1e).

### 2.2. Western blotting of transgenic silk fibroin

After the cocoons of the transgenic silkworms were degummed the transgenic silk fibroin was dissolved in 9 M LiBr aqueous solution at 37 °C. The solution was then dialyzed against distilled water for 3 days. The aqueous solution of transgenic silk fibroin was freeze dried to measure the concentration. SDS–PAGE gels and Western blotting with anti-GFP antibody of 50 mg $ml^{-1}$ transgenic silk fibroin aqueous solutions were observed. Similar experiments were performed for native silk fibroin as a comparison. GFP (Clontech Laboratories Inc., Tokyo, Japan) was used as a positive control. The GFP in the transgenic silk fibroin was detected using anti-GFP rabbit IgG (Invitrogen), horseradish peroxidase-conjugated anti-rabbit IgG antibody and TMB as the chromogenic substrate.

### 2.3. Ca binding activity assay of transgenic silk fibroin

The Ca binding activity of transgenic silk fibroin in aqueous solution was examined by modifying previous methods [33,34]. The experiment was started by adding 1.5 ml of 100 mM $CaCl_2$ solution to a mixture of 1.5 ml of 100 mM $NaHCO_3$ (pH 8.7) and 300 μl of the transgenic silk fibroin (10 mg $ml^{-1}$). $CaCO_3$ precipitation from the mixture of $CaCl_2$ solution and $NaHCO_3$ solution is prevented by the presence of transgenic silk fibroin. Since $CaCO_3$ has an absorption maximum at 570 nm, the rate of $CaCO_3$ precipitate formation can be monitored as the adsorption at 570 nm using a V-530 type UV–vis spectrometer (Jasco Inc., Japan). This $CaCO_3$ precipitation experiment is sensitive to pH and pH increases with time. Therefore, fresh $NaHCO_3$ solution (pH 8.7) was prepared in order to maintain the pH of the solution at 8.7. The Ca binding activity of native silk fibroin was also examined under the same experimental conditions.

X-ray photoelectron spectroscopy (XPS) was performed in order to obtain direct evidence of transgenic silk fibroin binding to Ca. Twenty microliters of an aqueous solution of transgenic silk fibroin was dropped on PVDF membrane (Bio-Rad, Tokyo, Japan), and the membrane immersed in a 1 mg $ml^{-1}$ $CaCl_2$ solution and then rinsed three times with 50% ethanol. The surface of the membrane was observed using a ESCA model 5400 (Ulvac PhaiI, Tokyo, Japan) with a Mg$K_\alpha$ source. The XPS images were recorded at a 45° take-off angle for the photoelectrons. The pass energy was 71.55 eV for narrow mode observations. XPS observations were also performed for native silk fibroin under the same experimental conditions as a comparison. In addition, complementary experiments were performed using Von Kossa staining for membranes with adsorbed silk protein prepared as above as follows. The membranes were immersed in 1% $AgNO_3$ aqueous solution for 40 min under UV irradiation and then rinsed in distilled water. They were then immersed in 3% $Na_2S_2O_3$ aqueous solution for 5 min and rinsed in distilled water. An image of the membrane was obtained with an Epson ES 8500scanner.

### 2.4. Scaffold preparation

Salt/water-derived transgenic silk fibroin porous scaffolds were prepared according to a previous method [35]. Briefly, salt particles were sieved through 300 and 500 μm meshes and packed into a plastic syringe. After the syringe had been filled with a 20 mg $ml^{-1}$ aqueous solution of transgenic silk fibroin the piston was depressed as quickly as possible to avoid a conformational change from random coil to β-sheet [35]. Air in the syringe was carefully eliminated. After the aqueous solution had been allowed to stand for 24 h silk/salt composites formed. These were immersed in distilled water to remove the salt. In order to observe the inner parts of the porous scaffolds a slice of the frozen scaffold was prepared using a razor blade. The pore shape and size in the slice was observed by scanning electron microscopy (VE-7800, Keyence, Osaka, Japan) at 1.2 keV. The average pore size was 425 μm.

### 2.5. Implantation to repair femoral defects

Japanese white rabbits (body weight 3.1 ± 0.2 kg, $n = 12$) were purchased from Japan SLC (Shizuoka, Japan). The rabbits were allowed free access to food and water ad libitum and were maintained under a 12 h light/dark cycle (lights on 8:00–20:00) at 23 ± 1 °C at 60 ± 10% humidity for 2 weeks before use. All rabbits were maintained and used in accordance with the guidelines for the Care and Use of Laboratory Animals of Nihon University School of Dentistry at Matsudo (08-0045). The rabbits were randomly assigned to one of three treatment groups. In Group I the defects were left empty (no implant control); in Group II the rabbits received silk scaffolds developed using native silk fibroin (native-SS); in Group III the rabbits received silk scaffolds developed with transgenic silk fibroin (trans-SS). Bone healing was monitored by radiography. The left femurs of the rabbits were scanned and four

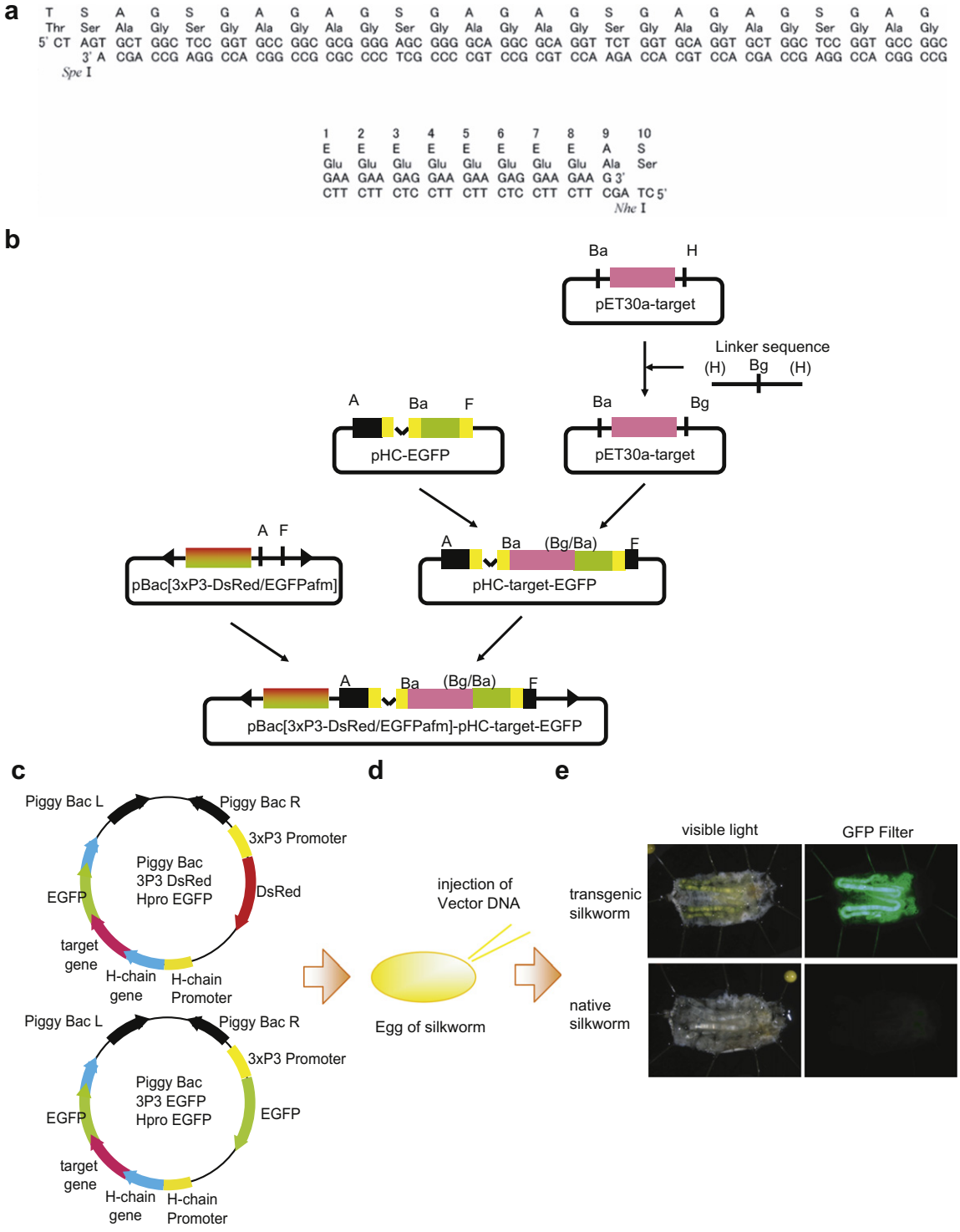


**Fig. 1.** (a) The designed oligonucleotide sequences for $E_8(AGSGAG)_4$. (b) Construction of the plasmids. Black boxes indicate the 5′-upstream and 3′-downstream regions of the *fibroin H* gene. Yellow boxes indicate the fibroin H coding region. Bent lines indicate intron sequences. Green boxes indicate the EGFP ORF. Red/green boxes indicate the 3xP3-DsRed/EGFP-poly(A) marker gene. (c) Physical map of piggy Bac-3xP3DsRed-H pro-(AGSGAG)4E8-EGFP. (d) Injection of DNA into eggs. (e) Appearance of the silk glands (upper, transgenic silkworm; lower, native silkworm) under bright field illumination (left) and through a GFP filter (right).

samples from each group were obtained after the animals were killed. All rabbits were injected intravenously with 25 mg $kg^{-1}$ sodium pentobarbital (Somnopentyl®, Kyoritsu Seiyaku, Tokyo, Japan). While the rabbits were under anesthesia the medial epicondyles of bilateral femurs were damaged (depth 6.0 mm) through the cortical bone surface into the cancellous bone, using an implant drill (diameter 3.6 mm, trephine bur, Micro Technology Co., Tokyo, Japan) along with physiological saline cooling (Fig. 2a). Fig. 2b shows a micro-CT image of the bone before it was damaged. Three left femoral defects were randomly filled with implant materials. After surgery each rabbit received an intramuscular injection of 50 mg $kg^{-1}$ sodium ampicillin (Viccillin®, Meiji, Tokyo, Japan). The rabbits were then returned to their cages and allowed to move freely. All wounds healed gradually. The rabbits were active and

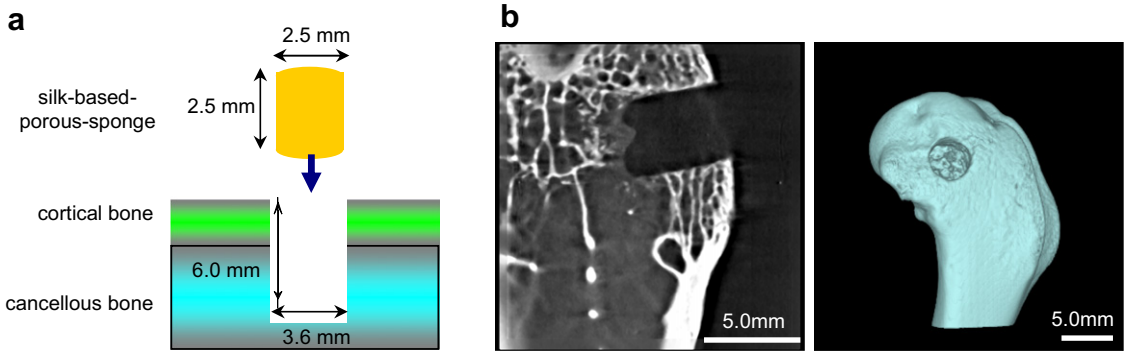


**Fig. 2.** (a) Bone defects (3.6 mm diameter, 6.0 mm depth) made through the cortical bone surface into the cancellous bone in the medial epicondyles of bilateral femora. (b) Micro-CT images (left, X-ray image; right, micro-CT image) of the initial state before filling with porous silk scaffolds.

without complications after surgery. A micro-CT system (Rigaku-mCT®, Tokyo, Japan) was used to examine the bones at 4 and 8 weeks after surgery, following which the rabbits were killed. Histological analysis was performed at 8 weeks.

### 2.6. Micro-CT

Quantitative analysis of the images of the newly grown bone was performed using an in vivo micro-CT system. After the rabbits were deeply anesthetized with intraperitoneally injected sodium pentobarbital (25 mg $kg^{-1}$) the rabbits were placed on the object stage one at a time. Rabbit femurs were scanned using a micro-CT system with an X-ray source of 90 kV per 88 μA at 4 and 8 weeks after surgery. Imaging of the rabbit femur was then performed over a full 360° rotation, with an exposure time of 2 min. An isotropic resolution of 30 × 30 × 30 μm voxel size was selected, which displayed the microstructure of the rabbit femora distal cortical bone and cancellous bone. The original three-dimensional (3-D) images were displayed and analyzed with I-View® software (J. Morita, Kyoto, Japan).

### 2.7. 3-D bone analysis for bone mineral content (BMC) and bone quantity (BV/TV)

The 3-D bone architecture at the femoral metaphysis was reconstructed and the structural indices of the femoral implant areas were calculated using a morphometric program (TRI/3D-BON, Ratoc System Engineering, Tokyo, Japan). A threshold value of 100 was used on the basis of previous studies [36,37]. In the 3-D analysis total volume (TV, $cm^3$), bone volume (BV, $cm^3$), and bone mineral content (BMC, mg) of the cancellous bone formed under the cortical bone were measured directly. The analyzed TV was measured in area of ϕ2.5mm, 2.5mm-height around defects. Volumetric density (BV/TV, %) was calculated from the BV and TV values. Among those indices, BV/TV (%) was evaluated in order to quantify the amount of new bone. All results are expressed as means ± SD. Data were analyzed using one-way ANOVA, followed by post hoc tests for pair-wise comparisons (Tukey's test). Differences were considered to be significant at $P < 0.05$.

### 2.8. Histological analysis

Rabbits were killed under anesthesia, using heart perfusion with physiological saline and 10% neutral formalin buffer solution, pH 7.4 (Wako, Tokyo, Japan), 8 weeks after surgery (three rabbits from each group). The specimens were fixed with 10% formalin for 72 h, decalcified in 10% EDTA (0.1 M phosphate buffer, pH 7.4) for 5 weeks, embedded in paraffin, and cut into 4 μm thick sections. The sections were stained with haematoxylin and eosin (H&E) and photographs were taken and evaluated under a light microscope.

### 2.9. $^{13}C$ CP/MAS NMR measurements

$^{13}C$ CP/MAS NMR experiments on transgenic silk fibroin and native silk fibroin scaffolds were performed in a Bruker DSX-400 Avance spectrometer with an operating frequency of 100.0 MHz for $^{13}C$.

The sample spinning rate was 7 kHz and mixing time was 2 ms. 30,000 scans were performed with a recycle delay of 3 s. The $^{13}C$ chemical shifts were represented relative to tetramethylsilane.

## 3. Results

### 3.1. Gene construction and expression of transgenic silk fibroin

A transformation vector, piggy Bac-3xP3 DsRed-H pro-$(AGSGAG)_4E_8$, was designed to produce recombinant fibroin that contained the fused gene with silk fibroin H-chain cDNA, $(AGSGAG)_4E_8$ and GFP sequences (Fig. 1b and c). Insertion of the plasmids was confirmed by digestion with *Bam*HI and *Bgl*II. Fig. 3a shows the results of electrophoresis through a 1.5% agarose gel; pET30a-$(AGSGAG)_4E_8$-Linker (lane 2), *Bgl*II digation of pET30a-$(AGSGAG)_4E_8$-Linker (lane 3), pHC-$(AGSGAG)_4E_8$-EGFP (lane 4), pBac [3xP3-EGFP afm]_pHC-$(AGSGAG)_4E_8$EGFP (lane 5), and pBac [3xP3-DsRed afm]_pHC-$(AGSGAG)_4E_8$EGFP (lane 6). They were 5500 and 500 (lanes 2 and 3), 870 (lane 4), and 2550 bp (lanes 5 and 6), respectively. These sizes were verified using PCR markers (lane 1). The DNA sequence was verified using a DNA sequencer. To construct transgenic silkworms, plasmid DNA was injected into 550 pre-blastodermal eggs of the w1-pnd strain (Fig. 1d). Transgenic insects were screened for expression of DsRed in the stemmata of $G_1$ embryos using a fluorescence microscope equipped with a filter set for DsRed. GFP fluorescence was observed in the posterior region of the silk gland and also in the cocoons (Fig. 1e). GFP fluorescence in the lumen of the silk gland and also in the cocoon indicates that the fused silk fibroins were produced in the silk gland, secreted into the lumen, and expelled into the cocoon, although the number of Ca binding sequences in the produced silk fibroin is small [32]. No fluorescence was detected in other tissues at any stage or in the silk glands of native silkworms.

The results of Western blotting for transgenic silk fibroin are shown in Fig. 3b. Western blotting using anti-GFP antibody exclusively detects GFP-tagged sequences in lane 2. The molecular weight of the sequence is expected to be 64 kDa, i.e. the sum of 37 kDa for $(AGSGAG)_4E_8$ and 27 kDa for GFP. The band detected was about 80 kDa, which was slightly higher than the expected value. A similar tendency has been observed in previous work on

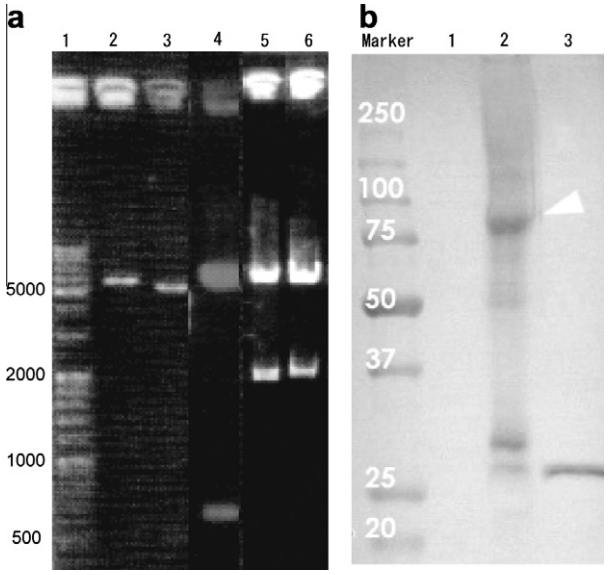


**Fig. 3.** (a) The results of the digestion analysis. Lanes 1, PCR markers; lane 2, pET30a-$(AGSGAG)_4E_8$-Linker; lane 3, *Bgl*II digation of pET30a-$(AGSGAG)_4E_8$-Linker; lane 4, pHC-$(AGSGAG)_4E_8$-EGFP; lane 5, pBac-[3xP3-EGFPafm]_pHC-$(AGSGAG)_4E_8$EGFP; lane 6, pBac-[3xP3-DsRed afm]_pHC-$(AGSGAG)_4E_8$EGFP. (b) Western blotting analysis of transgenic silk fibroin using anti-GFP antibody. Lane1, silk fibroin from native silkworm; lane 2, transgenic silk fibroin from transgenic silkworm; lane 3, GFP protein. The arrow shows the fibroin H-chain$(AGSGAG)_4E_8$-GFP fusion protein.

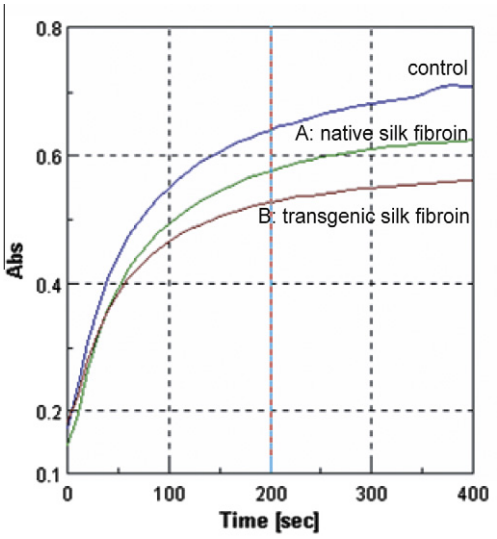


**Fig. 4.** Time dependencies of the peak intensity 570 nm absorbance of the aqueous solutions containing 1.5 ml of 100 mM $NaHCO_3$ (pH 8.7) and 0.3 ml (10 mg $ml^{-1}$) of native silk fibroin solution. (A) Green line, transgenic silk fibroin. (B) Red line, after addition of 1.5 ml of 100 mM $CaCl_2$ (pH 8.7). A similar experiment without silk fibroin was performed as a control.

transgenic silk fibroin [32] and $(AGSGAG)_4E_8$ produced by *E. coli* [28]. Takano et al. reported that the molecular weight tends to be slightly higher when the protein has a relatively high content of negatively charged amino acids [38]. The extra band around 27 kDa in Fig. 3b was thought to be due to an N-terminal domain fragment including the GFP tag removed during preparation of the silk fibroin solution.

### 3.2. Ca binding of transgenic silk fibroin

The inhibitory effect on the production of $CaCO_3$ is higher for transgenic silk fibroin compared with native silk fibroin (Fig. 4). This was expected due to the presence of poly-glutamic acid regions in the silk fibroin. However, this is indirect evidence. Therefore the following experiment was carried out to obtain direct evidence.

The element composition of transgenic silk fibroin adsorbed on the surface of a membrane after immersion in $CaCl_2$ solution was determined by XPS measurement, as shown in Fig. 5a. Two broad peaks, Ca 2p 3/2 (326.7 eV) and Ca 2p 1/2 (350.0 eV), were observed, characteristic of the presence of the Ca. The two peaks were also observed for silk fibroin, but the peak intensities were very low. Quantitative analysis of the intensities of the Ca 2p peaks was performed relative to the intensity of the C 1s peak. The intensity ratios Ca 2p/C 1s were 0.0134 for transgenic silk fibroin and 0.0031for native silk fibroin, respectively. These results indicate that the transgenic silk fibroin had a higher Ca binding activity than native silk fibroin. The higher Ca binding activity of transgenic silk fibroin compared with native silk fibroin was also shown by Von Kossa staining (Fig. 5b). Stronger staining was observed for the transgenic silk fibroin. Thus the introduction of poly-glutamic acid into silk fibroin in transgenic silkworms clearly promotes Ca binding.

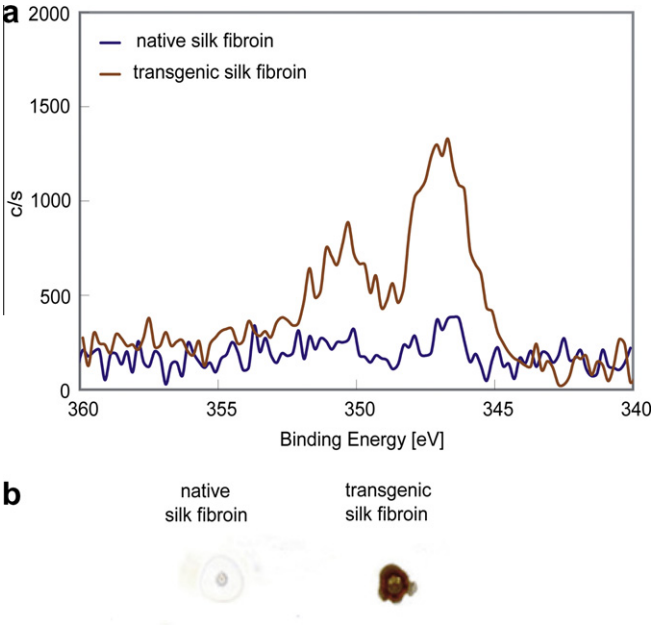


**Fig. 5.** (a) Narrow mode XPS Ca 2p spectra of transgenic silk fibroin (brown line) or native silk fibroin (blue line) adsorbed on membrane after immersion in $CaCl_2$ solution. The intensity of the C 1s peak. was used as a reference. (b) Von Kossa staining of transgenic silk fibroin or native silk fibroin adsorbed on membrane after immersion in $CaCl_2$ solution. (For interpretation of the references to colours in this figure legend, the reader is referred to the web version of this paper.)

### 3.3. Micro-CT examination and 3-D images

Typical micro-CT images of defects during the repair process are summarized in Fig. 6. Arrows indicate the positions of the initial defects. The white area in the X-ray images (left) shows mineralized bone, while the bright area in the micro-CT images (right) shows osteoid and bone. Comparing the images 4 and 8 weeks after surgery it can be seen that the brightness of the defect areas in Group III (trans-SS) increased gradually, indicating that new bone was being formed. In Group III the new bone began forming throughout the affected area 4 weeks after surgery, following which bone formation was rapid. Until 4 weeks after surgery the defect areas in all groups had similar depressions in the outer zones. After 8 weeks a depression in the cortical bone was observed in the defects of Group I but

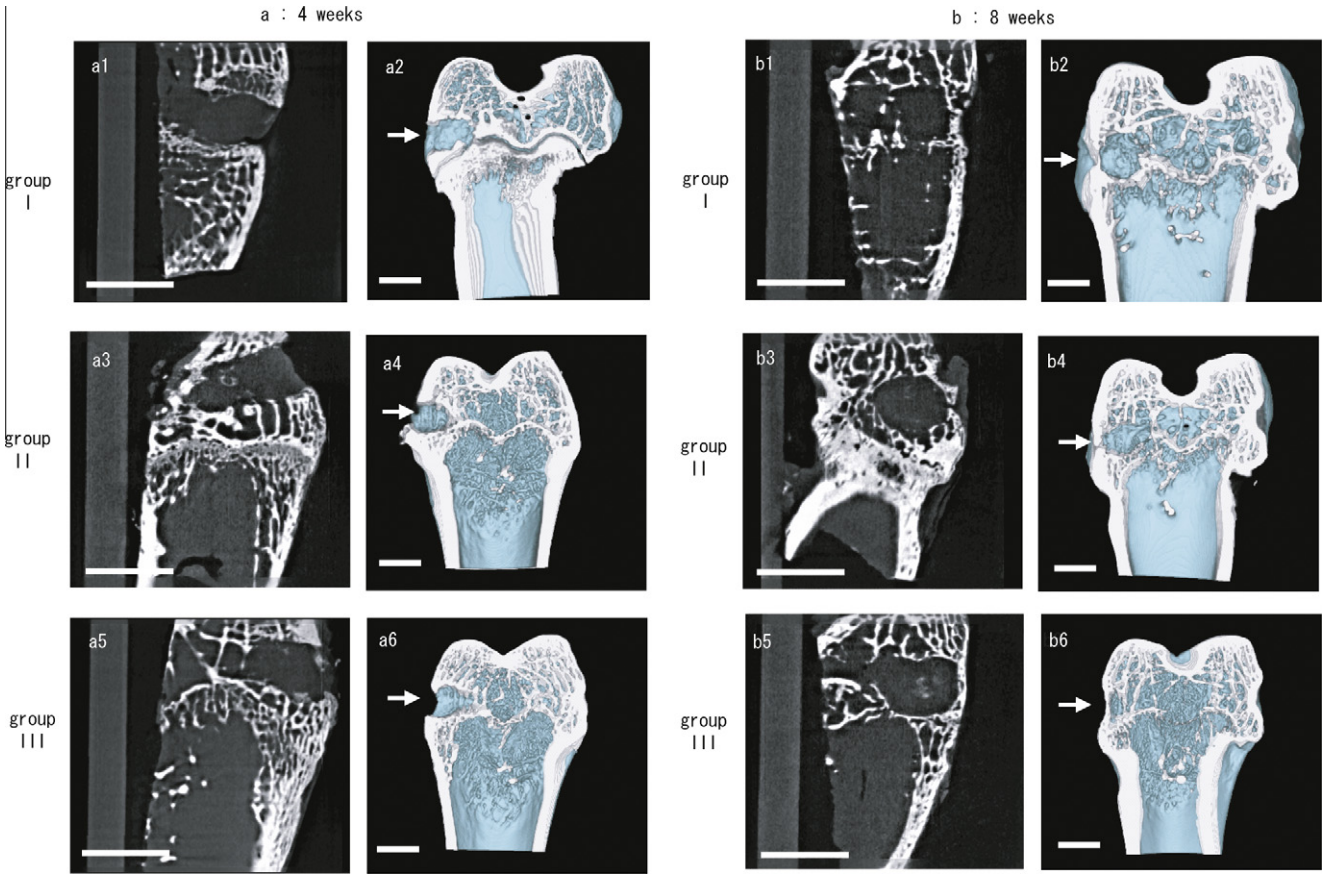


**Fig. 6.** Typical micro-CT images of defects during the repair process (a) 4 and (b) 8 weeks after surgery. The X-ray image (left) and micro-CT image (right) at 4 weeks are shown for Group I (a1 and a2), Group II (a3 and a4) and Group III (a5 and a6). The images at 8 weeks are also shown for Group I (b1 and b2), Group II (b3 and b4) and Group III (b5 and b6). The position of the defect is indicated by the arrow. Scale bar 5.0 mm.

not in the defects of Groups II and III. Groups II and III showed cortical-like bone in the outer zones and cancellous-like bone and irregular loosely connected bone tissue within the defect center.

### 3.4. BMC and BV/TV analyses

Fig. 7 shows quantitative analyses of the micro-CT images. The bone mineral content (BMC) is an indicator of the amount and mineralization of newly formed bone. 4 weeks after surgery the BMC (mg) in Groups I–III were 0.63 ± 0.23, 0.30 ± 0.05, and 1.36 ± 0.47, respectively, and after 8 weeks 1.64 ± 0.25, 2.05 ± 0.43, and 2.41 ± 0.28, respectively. Thus, with increasing time BMC increases for all groups as was expected. There are significant differences between Groups II and III after 4 weeks ($P < 0.05$). BMC clearly increases for Group III compared with Group II 4 weeks after surgery.

The quantity of new bone (BV/TV) in each group after 4 and 8 weeks is shown in Fig. 7b. BV/TV is an indicator of the relative amount of bone formed. 4 weeks after surgery BV/TV (%) in Groups I (control), II (native-SS), and III (trans-SS) were 6.9 ± 2.0, 4.4 ± 1.3, and 14.7 ± 5.3, respectively. 8 weeks after surgery BV/TV (%) in Groups I–III were 16.7 ± 3.1, 17.6 ± 3.6, and 18.7 ± 2.9, respectively. Thus, the BV/TV of trans-SS (Group III) was significantly higher after 4 weeks compared with that of native-SS (Group II) ($P < 0.05$). These result shows that defects treated with trans-SS (Group III) developed rapidly, with new bone being formed, compared with native-SS (Group II).

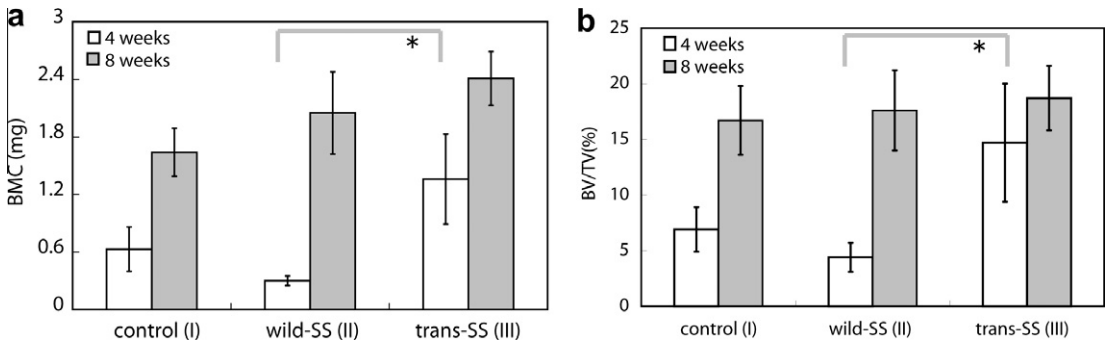


**Fig. 7.** Quantitative observations of bone formation using tomographic analysis. New bone quantity, BMC (a) and BV/TV (b) of each group at 4 (white) and 8 weeks (grey) after surgery. $^{*}P < 0.05$ in comparison with Group II.

### 3.5. Histological analysis (H&E staining)

The photomicrographs of H&E stained cross-sections of the femoral medial epicondyle bone defect sites of all groups 8 weeks after surgery are shown in Figs. 8 and 9. New bone formation was observed in defects with no implant (Group I) in the outer zone (marked area in Fig. 8a) after 8 weeks. No bone formation was observed inside the defects and there was a depression in the surface layer in Group I (Fig. 8a). This result corresponds to the depression of cortical bone seen in the micro-CT image (Fig. 6b2). Fig. 8b

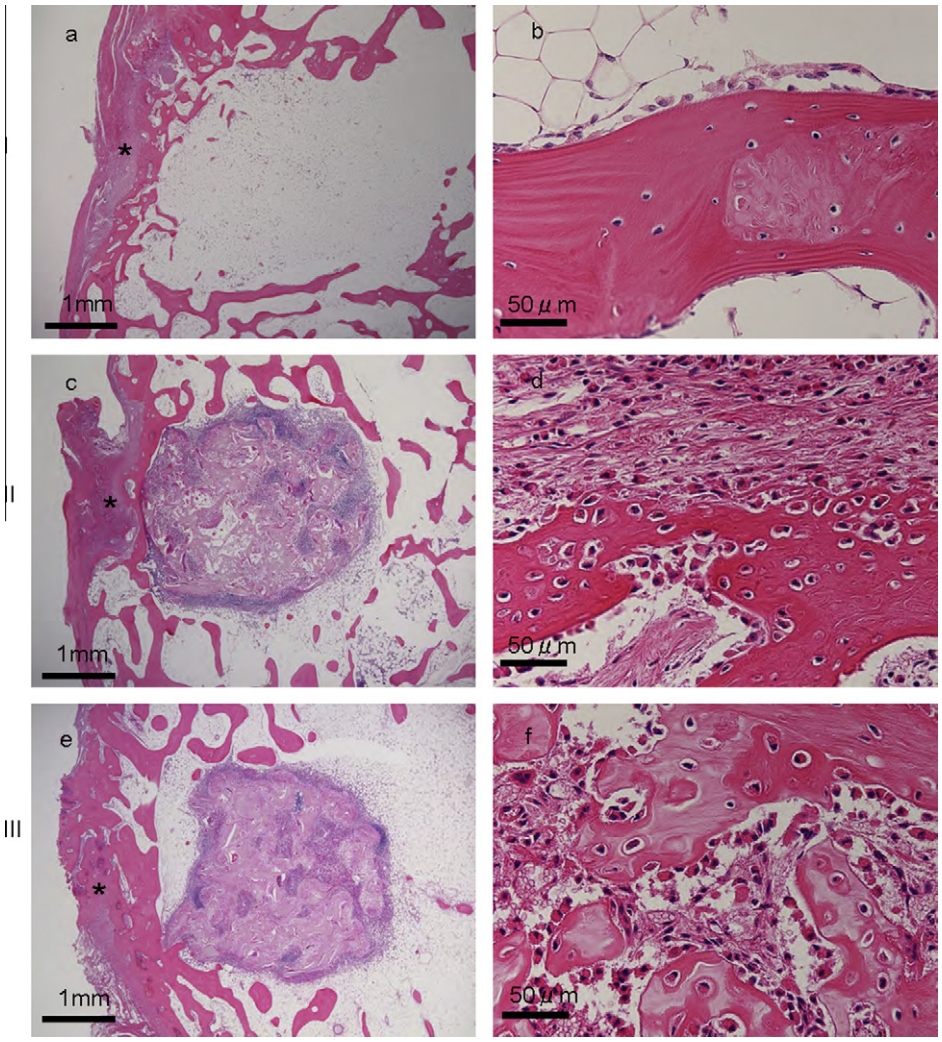


**Fig. 8.** Photomicrographs of H&E stained cross-sections through the femoral medial epicondyle bone defect sites at 8 weeks of Group I (a and b), Group II (c and d) and Group III (e, f). Expanded photomicrographs, (b), (d) and (f), are shown. These were selected from the surface (yellow point) of the bone layers, (a), (c) and (e), respectively.

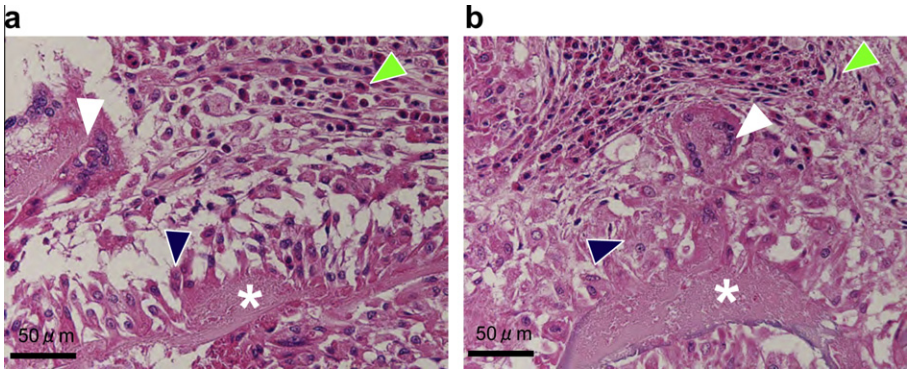


**Fig. 9.** Photomicrographs of H&E stained cross-sections at the surface of Group II (a) and Group III (b). Blue arrow, osteoblasts; white arrow, osteoclast; green arrows, infiltrating granulation tissue cells; asterisk, silk fibroin scaffold.

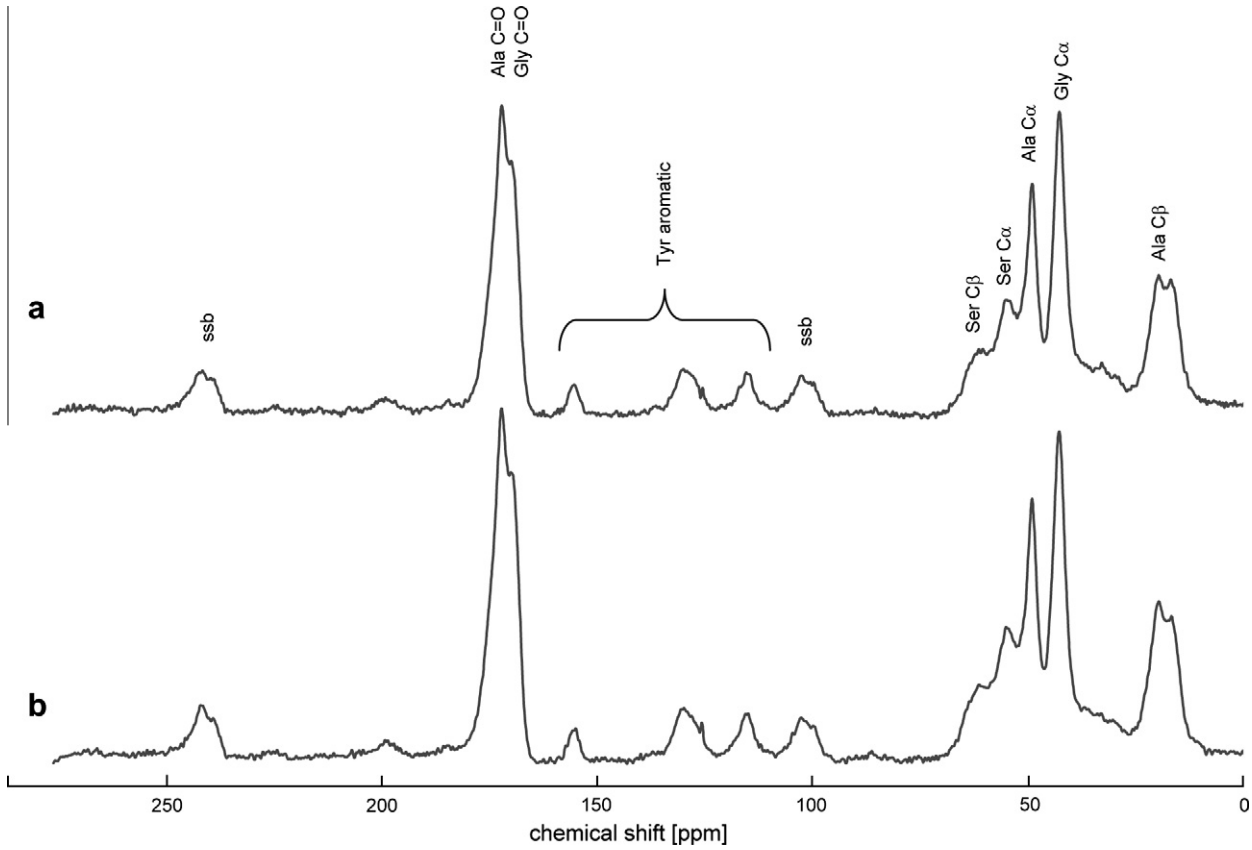


**Fig. 10.** $^{13}$C CP/MAS NMR spectra of (a) transgenic silk fibroin scaffold and (b) native silk fibroin scaffold, together with the assignments. Details of the experimental conditions are given in the text.

shows a magnified image of the outer zone seen in the area marked in Fig. 8a. Neonatal bone in the outer zone was composed of woven lamellar bone.

Defects treated with native-SS (Group II) and with trans-SS (Group III) had similar histological appearances (Figs. 8c and d and 9a (Group II) and Figs. 8e and f and 9b (Group III) at 8 weeks. Scaffolds were slightly substituted by newly formed bone (Fig. 8c and e). Granulation tissue invaded the silk fibroin scaffolds in Groups II and III, indicating that the silk fibroin scaffolds were phagocytosed by multinucleated cells and gradually absorbed, following which they were replaced by neonatal bone. New bone within the defect center, which was cancellous-like but irregular, because of repeated absorption and formation of bone, developed in Groups II (Fig. 8c) and III (Fig. 8e). Fig. 8d and f shows a magnified image of the outer zone marked in Fig. 8c and e, respectively. Fig. 8d and f shows that the outer zone is comprised of new cortical-like bone. No depression in the surface layer was observed because of volume maintenance by the silk fibroin scaffolds used in Groups II and III. This is consistent with the micro-CT results in Fig. 6b4 and b6, respectively.

The histology of the material surface in Groups II (Fig. 9a) and III (Fig. 9b) was analyzed in more detail. Asterisks indicate the silk fibroin sponge, blue arrows osteoblasts, white arrows osteoclasts, and green arrows infiltrating granulation tissue cells (Fig. 9a and b). Cells were identified from their morphology. Osteoblasts are mononuclear and lie along the periphery of bone during the formation of new bone. Osteoclasts are multinucleated giant cells. Inflammatory cells are mononuclear and form granulation tissue with fibroblasts. Photomicrographs show that osteoblast cells lay along the margins of the silk fibroin scaffolds in Groups II (Fig. 9a) and III (Fig. 9b). In the vicinity of the scaffold border both groups developed osteoblast layers, which are generally found randomly distributed with granulation tissue. These results indicate that the silk fibroin scaffolds were osteoinductive. Osteoclasts were also observed around the osteoblast layers. This indicates that neonatal bone formed around silk fibroin scaffolds through repetitive remodeling by osteoclasts and osteoblasts.

### *3.6. Structures of transgenic silk fibroin and native silk fibroin scaffolds in the solid state*

Finally, the structures of both scaffolds samples were examined by observing the $^{13}$C CP/MAS NMR spectra. The peak assignments have already been reported [29]. The chemical shifts change depending on the secondary structures of the protein in the solid state and, therefore, these will be a marker of the structure.

Fig. 10 shows that there is no significant change in the $^{13}$C CP/MAS NMR spectra, indicating no structural difference between the two silk proteins scaffolds.

## 4. Discussion

The micro-CT results (Fig. 6b4 and b6) were confirmed by the histological analysis results (Fig. 8c and e), which showed bone formation in Groups II and III 8 weeks after surgery. These results show that silk fibroin scaffolds provide adequate space and volume for tissue organization because they prevent depressions forming in the surface layer of a defect, however, Group II formed less bone than Group I after 4 weeks (Fig. 7). Group III showed markedly faster bone formation in the earlier stages, while also preventing depression formation. Previous studies have reported a need for mineralization on silk fibroin scaffolds with repetitive hydrophobic sequences for overall bone restoration in vivo [12]. Figs. 4 and 5

showed that the transgenic silk fibroin developed here had a high Ca binding activity in vitro because of the hydrophilic Ca-binding sites genetically introduced into hydrophobic H-chain of silk fibroin. Fig. 7 indicates that the Ca binding sequence $E_8(AGSGAG)_4$, transfected by transgenic engineering, promotes earlier osteogenesis through Ca binding (Figs. 4 and 5).

Fig. 9 indicates that neonatal bone formed through repetitive remodeling, i.e. bone matrix lysis by osteoclasts followed by bone formation by activated osteoblasts. Fig. 9a and b indicates that both native-SS- and trans-SS-treated surfaces showed bone forming activity by remodeling carried out by osteoclasts and osteoblasts. It is predicted that the genetically introduced Ca-binding sites in trans-SS affect both the remodeling and mineralization stages; osteoclasts adherent on the scaffold could lyse Ca-absorbed trans-SS, with osteoblasts being activated, as observed in bone remodeling. Activated osteoblasts on the trans-SS surface differentiate and ossify with deposited Ca. As a result, trans-SS forms bone earlier than native-SS because of its higher Ca binding activity (Fig. 7).

Poly-glutamic acid sequences or poly-aspartic acid sequences are present in HAP-nucleating proteins in native bone [16–26]. Focusing on this, Kim et al. prepared silk fibroin scaffolds by adding poly-aspartic acid sequences and then exposing the scaffolds to $CaCl_2$ and $NaHPO_4$. The CaP/silk composite scaffolds produced in this manner had improved osteoconductivity. However, they lacked the mechanical properties characterizing silks [10]. The silk-like protein developed here has hydrophilic Ca-binding sites that have been genetically introduced into the hydrophobic H-chain of silk fibroin. This study has shown that the Ca binding activities of genetically modified silk promotes early bone mineralization and bone restoration. Another approach for earlier bone regeneration is the acceleration of osteogenesis by supplying stem cells. In many studies of silk-based porous scaffolds successful bone repair has been achieved by providing bone marrow stem cells [7–10,12,13]. These studies have shown that mesenchymal stem cells (MSCs) can differentiate along an osteogenic lineage and that silk fibroin scaffolds seeded with MSCs show earlier mineralization than scaffolds without MSCs. Future studies should address the usefulness of our genetically modified silk scaffolds seeded with human MSCs.

## 5. Conclusions

Genetically modified silk containing poly-glutamic acid sites for mineralization was produced by transgenic silkworms. This silk had a high Ca binding activity. Porous silk fibroin scaffolds constructed using the silk produced by transgenic silkworms was implanted in rabbits. Earlier mineralization and bone formation was obtained with trans-SS than with native-SS. Thus, this study shows the feasibility of trans-SS as a mineralization-accelerating material for bone repair.

## Acknowledgements

T.A. acknowledges support with a Grant-in-Aid for Scientific Research from the Ministry of Education, Science, Culture and Supports of Japan (18105007) and a Grant for Supporting a Project of Strategic Research by the Ministry of Education, Culture, Sports, Science and Technology (2008-2012).

## Appendix A. Figures with essential colour discrimination

Certain figure in this article, particularly Figures 1, 2, 4–6, 8 and 9, is difficult to interpret in black and white. The full colour images can be found in the on-line version, at doi:10.1016/j.actbio.2010.10.032.

## References

[1] Reginster JY. The prevalence and burden of arthritis. Rheumatol Oxford 2002;41:3.
[2] McAndrew MP, Gorman PW, Lange TA. Tricalcium phosphate as a bone graft substitute in trauma: preliminary report. J Orthop Trauma 1988;2:333.
[3] Hollinger JO, Brekke J, Gruskin E, Lee D. Role of bone substitutes. Clin Orthop Relat Res 1996;324:55.
[4] Einhorn TA. Enhancement of fracture healing. J Bone Joint Surg An 1995;77:940–56.
[5] Bos GD, Goldberg VM, Zika JM, et al. Immune responses of rats to frozen bone allografts. J Bone Joint Surgery 1983;65:239.
[6] Athanasiou KA, Niederauer GG, Agrawal CM. Sterilization, toxicity, biocompatibility and clinical applications of polylactic acid/polyglycolic acid copolymers. Biomaterials 1996;17:93–102.
[7] Meinel L, Fajardo R, Hofmann S, et al. Silk implants for the healing of critical size bone defects. Bone 2005;37:688–98.
[8] Hofmann S, Hagenmller H, Koch AM, et al. Control of in vitro tissue-engineered bone-like structures using human mesenchymal stem cells and porous silk scaffolds. Biomaterials 2007;28:1152–62.
[9] Kim HJ, Kim UJ, Leisk GG, et al. Bone regeneration on macroporous aqueous-derived silk 3-D scaffolds. Macromol Biosci 2007;7:643–55.
[10] Kim HJ, Kim UJ, Kim HS, et al. Bone tissue engineering with premineralized silk scaffolds. Bone 2008;42:1226–34.
[11] Meechaisue C, Wutticharoenmongkol P, Waraput R, et al. Preparation of electrospun silk fibroin fiber mats as bone scaffolds. Biomed Mater 2007;2:181–8.
[12] Meinel L, Betz O, Fajardo R, et al. Silk based biomaterials to heal critical sized femur defects. Bone 2006;39:922–31.
[13] Meinel L, Karageorgiou V, Hofmann S, et al. Engineering bone-like tissue in vitro using human bone marrow stem cells and silk scaffolds. J Biomed Mater Res A 2004;71:25–34.
[14] Hutmacher DW. Scaffolds in tissue engineering bone and cartilage. Biomaterials 2000;21:2529–43.
[15] Zhou CZ, Confalonieri F, Medina N, et al. Fine organization of *Bombyx mori* fibroin heavy chain gene. Nucleic Acids Res 2000;28:2413.
[16] Xu L, Anderson AL, Lu Q, Wang J. Role of fibrillar structure of collagenous carrier in bone sialoprotein-mediated matrix mineralization and osteoblast differentiation. Biomaterials 2007;28:750–61.
[17] Hunter GK, Goldberg HA. Modulation of crystal formation by bone phosphoproteins: Role of glutamic acid-rich sequences in the nucleation of hydroxyapatite by bone sialoprotein. Biochem J 1994;302:175.
[18] Hunter GK, Kyle CL, Goldberg HA. Modulation of crystal formation by bone phosphoproteins: structural specificity of the osteopontin-mediated inhibition of hydroxyapatite formation. Biochem J 1994;300:723.
[19] Harris NL, Rattray KR, Tye CE, et al. Functional analysis of bone sialoprotein: identification of the hydroxyapatite-nucleating and cell-binding domains by recombinant peptide expression and site-directed mutagenesis. Bone 2000;27:795–802.
[20] Stubbs JT, Mintz KP, Eanes ED, Torchia DA, Fisher LW. Characterization of native and recombinant bone sialoprotein: delineation of the mineral-binding and cell adhesion domains and structural analysis of the RGD domain. J Bone Miner Res 1997;12:1210–22.
[21] Ganss B, Kim RH, Sodek J. Bone sialoprotein. Crit Rev Oral Biol Med 1999;10:79.
[22] Lian JB, Glimcher MJ, Roufosse AH, et al. Alterations of the gamma-carboxyglutamic acid, osteocalcin concentrations in vitamin D-deficient chick bone. J Biol Chem 1982;257:4999.
[23] Roach HI. Why does bone matrix contain non-collagenous proteins? The possible roles of osteocalcin, osteonectin, osteopontin and bone sialoprotein in bone mineralisation and resorption. Cell Biol Int 1994;18:617–28.
[24] Robey PG, Fisher LW, Young MF, Termine JD. The biochemistry of bone. Osteoporosis Etiol Diagn Manage 1988;2:95–109.
[25] Boskey AL. Osteopontin and related phosphorylated sialoproteins: effects on mineralization. Ann NY Acad Sci 1995;760:249.
[26] Hunter GK, Goldberg HA. Nucleation of hydroxyapatite by bone sialoprotein. Proc Nat Acad Sci 1993;90:8562.
[27] Haber-Pohlmeier S, Abarca-Heidemann K, Körschen HG, et al. Binding of $Ca^{2+}$ to glutamic acid-rich polypeptides from the rod outer segment. Biophys J 2007;92:3207–14.
[28] Nagano A, Sato H, Tanioka T, et al. Characterization of Ca binding-amphipathic silk-like protein and peptide with the sequence,$(Glu)_8$(Ala-Gly-Ser-Gly-Ala-Gly)$_4$ for bone repair biomaterials. Submitted for publication.
[29] Nagano A, Kikuchi Y, Sato H, et al. Structural characterization of silk-based water-soluble peptides $(Glu)_n$(Ala-Gly-Ser-Gly-Ala-Gly)$_4$ ($n$ = 4–8) as a mimic of *Bombyx mori* silk fibroin by $^{13}C$ solid-state NMR. Macromolecules 2009;42:8950–8.
[30] Tamura T, Thibert T, Royer C, et al. A piggybac element-derived vector efficiently promotes germ-line transformation in the silkworm *Bombyx mori*. Nat Biotechnol 2000;18:81–4.

[31] Kojima K, Kuwana Y, Sezutsu H, et al. A new method for the modification of fibroin heavy chain protein in the transgenic silkworm. Biosci Biotechnol Biochem 2007;71:2943–51.
[32] Yanagisawa S, Zhu Z, Kobayashi I, et al. Improving cell-adhesive properties of recombinant *Bombyx mori* silk by incorporation of collagen or fibronectin derived peptides produced by transgenic silkworms. Biomacromolecules 2007;8:3487–92.
[33] Inoue H, Ozaki N, Nagasawa H. Purification and structural determination of a phosphorylated peptide with anti-calcification and chitin-binding activities in the exoskeleton of the crayfish, Procambarus clarkii. Biosci Biotechnol Biochem 2001;65:1840–8.
[34] Hidaka S, Matsuo T, Ouchi K. A method for testing the salivary ability against the formation of calcium phosphate precipitates. J Dental Health 2003;53:137–44.
[35] Makaya K, Terada S, Ohgo K, Asakura T. Comparative study of silk fibroin porous scaffolds derived from salt/water and sucrose/hexafluoroisopropanol in cartilage formation. J Biosci Bioeng 2009;108:68–75.
[36] Ito M, Nishida A, Koga A, et al. Contribution of trabecular and cortical components to the mechanical properties of bone and their regulating parameters. Bone 2002;31:351–8.
[37] Hahn M, Vogel M, Pompesius-Kempa M, Delling G. Trabecular bone pattern factor–a new parameter for simple quantification of bone microarchitecture. Bone 1992;13:327–30.
[38] Takano E, Maki M, Mori H, et al. Pig heart calpastatin: Identification of repetitive domain structures and anomalous behavior in polyacrylamide gel electrophoresis. Biochemistry 1988;27:1964–72.